Computational characterization of micro- to mesoscopic deformation behavior of semicrystalline polymers

Tomita, Yoshihiro

Uchida, Makoto

Computational Characterization of Micro- to Mesoscopic Deformation Behavior of Semicrystalline Polymers

Yoshihiro Tomita and Makoto Uchida

Graduate School of Science and Technology, Kobe University

Abstract

In the present study, we clarify the micro- to mesoscopic deformation behavior of semicrystalline polymers by the finite element homogenization method. The crystalline plasticity theory using a penalty method for the inextensibility constraint in the chain direction and the nonaffine molecular chain network theory were used to the representation of the deformation behavior of crystalline and amorphous phases, respectively, in the composite microstructure of a semicrystalline polymer. Various directional tensions are applied to the two dimensional plane-strain unit cell model of a composite microstructure. The results reveal a highly anisotropic deformation behavior caused by the rotation of the chain direction and lamella interface, which depends on tensile direction and manifests as substantial hardening/softening in the early stage of deformation. The mesoscopic structure of a semicrystalline polymer was modeled using a voronoi polygon comprised of composite microstructures with different lamella interface directions. The initial isotropy of the response of the mesoscopic scale was verified. Due to their interaction with the surrounding grains, the individual grains of the mesoscopic scale show a conservative response as compared with that of the unit cell, and a very nonuniform response depending on the location of the respective grain is observed; these are typical of the mesoscopic response of semicrystalline polymers.

Corresponding Address:
Professor Yoshihiro TOMITA
Department of Mechanical Engineering
Faculty of Engineering, Kobe University
1-1, Rokkodai-cho, Nada Kobe 657-8501, JAPAN
Tel:+81-78-803-6125 Fax: +81-78-803-6155
email: tomita@mech.kobe-u.ac.jp
URL: http://solid.mech.kobe-u.ac.jp

1. Introduction

To enable the wide use of semicrystalline polymers as structural materials, the characterization of their mechanical behaviors is indispensable. Semicrystalline polymers have a very complex hierarchical structure, and their microstructures are that of a two-phase composite material consisting of a crystalline lamella and an amorphous layer. In the crystalline phase, molecular chains are oriented in a specific direction along with an enforced inextensibility. Spherulite is formed with a radial arrangement of broad thin lamellae. Although the deformation mechanisms of the microstructure strongly depend on the directions of the molecular chains and lamella interface, macroscopic deformation behavior still exhibits initial isotropy [1].

In accordance with the above characteristics of semicrystalline polymers, simplified models have been proposed to reproduce experimental results [2], [3]. In these studies, interaction laws based on the Taylor, Sachs and self-consistent models were employed to relate microscopic and macroscopic deformations. The initially isotropic response by modeling the aggregation of randomly oriented composite microstructures is realized. However, these models cannot be used in evaluating the interactions between adjacent composite phases which exhibit a largely scattered local rotation and deformation of lamellae in the mesoscopic scale, as clarified by AFM observation, depending on the initial orientation of the lamellae and deformation due to applied deformation [4]. Therefore these characteristic deformation behaviors on the micro- to mesoscopic scales are essential in evaluating the local deformation behavior of semicrystalline polymers.

Here, we focus our attention to the mesoscopic modeling of the semicristalline polymer that has a patchworklike structure with different directions of the lamella interface [5]. Therefore, we will first provide constitutive equations for individual phases, namely, crystalline and amorphous phases. Subsequently, we introduce the unit cell model comprised of crystalline and amorphous phases with different volume fractions. The deformation behavior of a unit cell is evaluated by a large-deformation finite element homogenization method [6]. With regard to the mesoscopic structure, experimental observation suggests the existence of the patchworklike structure where the lamella interface has almost the same direction in each patchwork domain with several to several dozens of μm square [5]. Based on this experimental evidence, we will generate the mesoscopic structure using a voronoi

polygon comprised of composite microstructures with different lamella interface directions. The constitutive equation at each material point of the voronoi polygon is assigned using the homogenized constitutive equation of unit cell. Thus, we will evaluate the interaction between such microstructures and the heterogeneous deformation behavior on the micro- to mesoscopic scales.

2. Constitutive Equation

Here, in order to describe the deformation behavior of semi-crystalline polymer, the crystalline plasticity theory [7] with the penalty method to introduce inextensibility of the chain direction and the nonaffine molecular chain network theory [8] are employed for crystalline and amorphous phases, respectively.

The total strain rate d_{ij} is assumed to be decomposed into the elastic strain rate d_{ij}^e and plastic strain rate d_{ij}^p. With Hooke's law for the elastic strain rate d_{ij}^e, the constitutive equation that relates the rate of Kirchhoff stress $\dot{S}_{ij}$ to strain rate d_{ij} becomes

$$d_{ij} = d_{ij}^e + d_{ij}^p, \quad \dot{S}_{ij} = D_{ijkl}^e d_{kl}^e - F_{ijkl} d_{kl}, \quad F_{ijkl} = \frac{1}{2}\left(\sigma_{ik}\delta_{jl} + \sigma_{il}\delta_{jk} + \sigma_{jl}\delta_{ik} + \sigma_{jk}\delta_{il}\right), \tag{1}$$

where D_{ijkl}^e is the elastic stiffness tensor and σ_{ij} is the Cauchy stress.

The plastic strain rate d_{ij}^p in the crystalline phase is modeled using the crystalline plasticity theory [7], with shear strain rate $\dot{\gamma}_{pv}^{(\alpha)}$ on the α th slip system expressed by a power law [9], as

$$d_{ij}^p = \sum_{(\alpha)} P_{ij}^{(\alpha)} \dot{\gamma}_{pc}^{(\alpha)}, \quad \dot{\gamma}_{pc}^{(\alpha)} = \dot{\gamma}_{0c} \frac{\tau^{(\alpha)}}{g^{(\alpha)}} \left| \frac{\tau^{(\alpha)}}{g^{(\alpha)}} \right|^{\frac{1}{m}-1}, \tag{2}$$

where $\dot{\gamma}_{0c}$ is the reference strain rate in the crystalline phase, m is the strain rate sensitivity exponent, $g^{(\alpha)}$ is the resistance to slip, $\tau^{(\alpha)} = P_{ij}^{(\alpha)} \sigma_{ij}$ is the resolved shear stress, $P_{ij}^{(\alpha)} = (s_i^{(\alpha)} m_j^{(\alpha)} + m_i^{(\alpha)} s_j^{(\alpha)})/2$ is the Schmid tensor, and $s_i^{(\alpha)}$ and $m_i^{(\alpha)}$ are unit vectors along the slip direction and the slip plane normal, respectively. Here, the penalty method is employed to approximately satisfy the inextensibility of the chain direction. The corresponding constitutive equation of the crystalline phase is expressed as [10]

$$\dot{S}_{ij} = \left(D^e_{ijkl} - F_{ijkl} - E_c c_i c_j c_k c_l\right) d_{kl} - \sum_{(\alpha)} R^{(\alpha)}_{ij} \dot{\gamma}^{(\alpha)}_{pc},$$
$$R^{(\alpha)}_{ij} = D^e_{ijkl} P^{(\alpha)}_{kl} + \left(W^{(\alpha)}_{ik}\sigma_{kj} + \sigma_{ik} W^{(\alpha)}_{kj}\right)\dot{\gamma}^{(\alpha)}_{pc}, \quad \mathrm{W}^{(\alpha)}_{\mathrm{ij}} = \frac{1}{2}\left(s^{(\alpha)}_{i} m^{(\alpha)}_{j} - m^{(\alpha)}_{i} s^{(\alpha)}_{j}\right) \tag{3}$$

where E_c is the penalty constant which has a large value, and physically, it represents the chain directional stiffness. c_i is the unit vector of chain direction.

Subsequently, the plastic strain rate d^p_{ij} in the amorphous phase is modeled using a nonaffine eight-chain model [8], with plastic shear strain rate $\dot{\gamma}_{pa}$ [11], as

$$d^p_{ij} = \frac{\dot{\gamma}_{pa}}{\sqrt{2}\tau^*}\hat{\sigma}'_{ij}, \quad \tau^* = \left(\hat{\sigma}'_{ij}\hat{\sigma}'_{ij}\right)^{\frac{1}{2}}, \quad \hat{\sigma}_{ij} = \sigma_{ij} - B_{ij}, \quad \dot{\gamma}_{pa} = \dot{\gamma}_{0a}\exp\left[\left(-\frac{A\tilde{s}}{T}\right)\left\{1 - \left(\frac{\tau^*}{\tilde{s}}\right)^{\frac{5}{6}}\right\}\right], \tag{4}$$

where $\dot{\gamma}_{0a}$ and A are constants, T is the absolute temperature, τ^* is the applied shear stress, $\tilde{s} = s_0 + \alpha p$, $s_0 = 0.077\mu/(1-\nu)$ is the athermal shear strength [12], p is the pressure, and α is a pressure-dependent coefficient. Furthermore, B_{ij} in Eq. (4) is the back-stress tensor and the principal components b_i are expressed, by employing the eight-chain model [13], as

$$b_i = \frac{1}{3}C^R\sqrt{N}\frac{V_i^2 - \lambda^2}{\lambda}\mathrm{L}^{-1}\left(\frac{\lambda}{\sqrt{N}}\right), \tag{5}$$

where $\lambda^2 = (V_1^2 + V_2^2 + V_3^2)/3$, V_i is the principal plastic stretch, N is the average number of segments in a single chain, $C^R = nk_BT$ is a constant, n is the number of chains per unit volume, k_B is Boltzmann's constant, and $\mathrm{L}(x) = \coth(x) - 1/x$ is the Langevin function. In the nonaffine eight-chain model [8], the change in the number of entangled points, in other words, the average number of segments N, may change depending on the distortion ξ which represents the local deformation of a polymeric material [8]. The simplest expression of the number of entangled points is $N = N_0\exp\{c(1-\xi)\}$ with $\xi = 1$ in the reference state, and N_0 is the number of segments in a single chain in the reference state and c is a material constant.

3. Computational Model

In order to establish the multiscale model of semicrystalline polymer, the lamella like micro structure comprised of crystalline and amorphous phases is assumed to be distributed periodically at the material point of mesoscopic scale as indicated in Fig.1, the homogenization method for large elastoviscoplastic deformation behavior [6], [15] is employed. The crystalline structure of HDPE exhibits orthorombic structure which has four chain slip directions where inextensibility constrain is enforced and four transverse slip directions perpendicular to the chain directions.

Figure 1 (a) illustrates a hypothetical plane strain computational unit cell model in which crystalline and amorphous phases are assumed to be stacked periodically. To represent micro- to mesoscopic deformation behavior, we employ the homogenization method [6]. For a two-dimensional simulation, 2 slip systems, namely the chain slip and the transverse slip, are modeled, and the coherent boundary condition is applied to the lamella interface. The misalignment of the chain direction and lamella interface direction is $\theta_{c0} - \theta_{i0} = 120^{\circ}$, as indicated in Fig. 1(a) [2].

For the mesoscopic scale, an experimental observation suggested the presence of a patchworklike structure with several to several dozens of μm square, on the plane with a normal parallel to the radial direction of spherulite. In each patchwork region, the lamella interfaces have almost the same direction. Therefore, we approximated this characteristic feature by introducing voronoi polygons as indicated in Fig. 1(b) and assign the interface angle θ_{i0} randomly. The initial distribution of interface directions is determined such that we generated random numbers corresponding to the total number of polygons and specified the corresponding direction of the interface, and allocated the angle to each grain. Fig. 1(b) shows the distribution of angles on the mesoscopic scale.

Each material point of the polygon, that is, finite element, obeys the homogenized constitutive equation of semi-crystalline unit cells as indicated in Fig. 1(a). Here, to capture the essential feature of the mesoscopic scale, the distribution of the initial shear strength [14] was disregarded. In such case, the unit cell under the periodic boundary condition deforms uniformly; therefore, very coarse mesh discretizations are acceptable without the loss of generality.

For the representation of stress state and deformation, we introduce equivalent stress

and strain rate for a material point as $\dot{\varepsilon}_{eq}^2 = 2d_{ij}d_{ij}/3$, $\sigma_{eq}^2 = 3\sigma_{ij}^{\circ}\sigma_{ij}^{\circ}/2$, for the unit cell as $\dot{E}_{eq}^2 = 2\dot{E}_i\,\dot{E}_i/3$, $\Sigma_{eq}^2 = 3\Sigma_i^{\circ}\Sigma_i^{\circ}/2$, for an average value of a single grain as $\dot{\widetilde{E}}_{eq}^2 = 2\dot{\widetilde{E}}_i\,\dot{\widetilde{E}}_i/3$, $\widetilde{\Sigma}_{eq}^2 = 3\widetilde{\Sigma}_i^{\circ}\widetilde{\Sigma}_i^{\circ}/2$ and for an average value of the mesoscopic scale as $\dot{\overline{E}}_{eq}^2 = 2\dot{\overline{E}}_i\,\dot{\overline{E}}_i/3$, $\overline{\Sigma}_{eq}^2 = 3\overline{\Sigma}_i^{\circ}\overline{\Sigma}_i^{\circ}/2$. Here, $\dot{E}_i$ and Σ_i' are the homogenized strain rate and deviatoric part of stress Σ_i over a unit cell, $\dot{\widetilde{E}}_i$ and $\widetilde{\Sigma}_i'$ are the average strain rate and deviatoric part of stress $\widetilde{\Sigma}_i$ over a single grain, and $\dot{\overline{E}}_i$ and $\overline{\Sigma}_i'$ are the average strain rate and deviatoric part of stress $\overline{\Sigma}_i$ over a mesoscopic scale, respectively. Similarly, $\sigma_m = \sigma_{ii}/3$, $\Sigma_m = (\Sigma_1 + \Sigma_2 + \Sigma_3)/3$, $\widetilde{\Sigma}_m = (\widetilde{\Sigma}_1 + \widetilde{\Sigma}_2 + \widetilde{\Sigma}_3)/3$ and $\overline{\Sigma}_m = (\overline{\Sigma}_1 + \overline{\Sigma}_2 + \overline{\Sigma}_3)/3$ represent the mean stress for a material point and a unit cell, and the average mean stress of the single crystal and that of the mesoscopic scale, respectively.

The material parameters are specified in refs. [2], [3] and [8]. For the amorphous phase, $E_{Amo}/s_0 = 23.7$, $As_0/T = 58.3$, $\alpha = 0.01$, $\dot{\gamma}_{0a} = 1\times10^{16}/\mathrm{s}$, $s_0 = 71.9\mathrm{MPa}$, $C_R/s_0 = 0.07$, $\sqrt{N_0} = 2.83$ and $c = 0.33$; for the crystalline phase, $E_{Cry}/g^{(c)} = 125$, $\dot{\gamma}_{0c} = 1\times10^{-3}/\mathrm{s}$, $g^{(c)} = 8.0\mathrm{MPa}$, $g^{(t)} = 2.5g^{(c)}$ and $1/m = 9$ are employed at $T = 296\mathrm{K}$. Here, the superscripts (c) and (t) represent the chain slip and transverse slip, respectively. Furthermore, to sufficiently reproduce inextensibility and to carry out stable calculation, the penalty constant $E_c = 10^6$ MPa is employed.

Mesoscopically homogeneous deformations are applied by prescribing the strain rate $\dot{E}_2 = \dot{\overline{E}}_2 = \dot{E}_0 = 10^{-5}/s$ and stress rate $\dot{\Sigma}_1 = \dot{\overline{\Sigma}}_1 = 0$ with respect to the coordinates x_1 and x_2, respectively. The rotation of the unit cell is evaluated by that of the coordinates y_1 and y_2.

4. Results and Discussion

4.1 Deformation Behavior of Unit Cell

Figure 2 indicates the relationship between (a) equivalent stress Σ_{eq}, (b) direction of chain axis θ_c, and (c) direction of lamella interface θ_i and equivalent strain E_{eq} for unit cell under various directional tensions with $\theta_{i0} = 0^\circ, 30^\circ, 60^\circ, 90^\circ, 120^\circ$ and 150°. Here, the volume fraction of the crystalline phase is fixed at 0.5. According to Fig.2 (a), deformation responses

represents high anisotropy, which is attributable to preferential slip of the chain slip system in the crystalline phase which has a lower resistance of slip than that of transverse slip systems, and misalignment of lamella interface and chain directions. Chain and lamella interface directions rotate to the tensile direction as deformation increases. Due to the orientation of the chain direction in the tensile direction, the stiffness of the crystalline phase is increased by the inextensibility of the chain direction. Furthermore, the rotation of the lamella interface direction to the tensile direction causes the increase of equivalent stress because the crystalline phase supports the deformation resistance of the overall unit cell. In the case of $\theta_{i0} = 30^\circ$, equivalent stress decreases at $E_{eq} \cong 0.25$. When the chain direction rotates from the initial state ($\theta_c = 150^\circ$) to the tensile direction, the chain direction aligns the 135° which is the maximum shear stress direction. Then, the shear stress on chain slip rises beyond prior state while the slip resistance does not increase. As a result, softening occurs in the crystalline phase.

Figure 3 indicates mean stress Σ_m in (a) amorphous phase and (b) that in crystalline phase vs. equivalent strain E_{eq} for unit cell. Because each phase is assumed to be layered infinitely in a unit cell, uniform deformation occurs in each phase. Regardless of the tensile directions, mean stress in the amorphous phase exhibits a higher value than that in the crystalline phase in a later stage of deformation. In the case of $\theta_{i0} = 0^\circ$, compressive deformation along the direction normal to the tensile deformation in the amorphous phase is strongly prescribed by the hardened crystalline phase, and which causes a substantial increase of mean stress in the amorphous phase. This suggests the onset of stress concentration in a region where the lamella interface normal is in the loading direction at the initial stage of deformation; this may lead to microscopic fractures. The same situation may occur in semi-crystalline polymer.

Figure 4 indicates the deformation behavior of a two-phase composite microstructure at different degrees of deformation for $\theta_{i0} = 0^\circ, 30^\circ, 90^\circ$, and 150°. These results also indicate the completely different deformation behavior depending on the initial direction of the lamella interface. For example, in the results for $\theta_{i0} = 30^\circ$ and $\theta_{i0} = 150^\circ$, the lamella interface direction is symmetric with respect to the tensile direction but the chain directions in the crystalline phase are 150° and 90°, respectively, which leads to a marked difference in plastic deformation behavior and reflects the stress-strain relations in Fig. 2(a). Thus the deformation

behavior of single crystals of semicrystalline polymers exhibits a strong anisotropy depending on lamella interface direction, which implies that the single crystals interact with the surrounding crystals with different directional lamella interfaces to satisfy the equilibrium and compatibility conditions. This suggests the need for a suitable mesoscopic model that will account for such interaction between the grains.

4.2 Deformation Behavior of Mesoscopic Scale

Here the micro- to mesoscopic deformation behavior of semicrystalline polymers will be presented. Generally, the volume fraction of the crystalline phase is assumed to be 50%. Initially, we will clarify the deformation behavior of the mesoscopic scale. An initial isotropy of the model was examined by using a tension in two directions. Figure 5 indicates the relationships between the average equivalent stress $\overline{\Sigma}_{eq}$ and the strain $\overline{E}_{eq}$ in mesoscopic scale for the tension indicated in Fig. 1(b) and that rotated clockwisely by 90°. Regardless of the tension directions, the responses are almost identical; therefore, the isotropic response of the mesoscopic scale in the small to large strain range has been essentially assured. The nonlinear behavior prior to mesoscopic yielding is attributable to the different magnitudes of resolved shear stress in the chain slip direction, which causes the yielding in the different stages of deformation. Figure 6 indicates the effect of the volume fraction of the crystalline phase on the average equivalent stress $\overline{\Sigma}_{eq}$ and strain $\overline{E}_{eq}$ relations for the mesoscopic scale. The effect of crystallinity on the stress-strain relations in the low strain regions is predominant and elasticity modulus is very sensitive to the volume fraction of crystalline phase, which is intensified by enhancing crystallization. This stress-strain behavior is the homogenized behavior of individual grains exhibiting quite different responses as indicated in section 4.1 under the interaction of the surrounding grains.

Figure 7 indicates the equivalent strain rate $\dot{\varepsilon}_{eq} / \dot{E}_0$ distributions at (1)-(5) in the stress-strain relations shown in Fig. 5. The magnitude of the strain rate is normalized by the average value of the mesoscopic scale $\dot{E}_0$. Due to orientation hardening in the amorphous and crystalline phases and the rotation of the lamella interface direction, mesoscopically localized deformation regions intersecting grains propagate to the remaining region. The highly nonuniform deformation accompanied by the onset and propagation of very localized deformations in specific grains is observed. These are the results of the interaction between the grains and the direction of the lamella interface. Figure 8 shows the deformation behavior

of four different material points, A, B, C and D, in Fig. 7(1). Points A and B have approximately similar lamella interface directions. The material points in the mesoscopic scale with similar microstructures exhibit quite different deformation behaviors, which are closely associated with the interaction with the surrounding crystal. The AFM observation of the rotation of lamella in the mesoscopic scale of high-density polyethylene (HDPE) under tension indicates that the material points essentially rotate in accordance with the rotation of the mesoscopic scale with a very large fluctuation [4]. The present computational simulation is not necessarily the model of the HDPE employed in the experimental work, however, similar tendencies of the local deformation behavior of the lamella with different directions were observed.

Figure 9 indicates average equivalent stress $\overline{\Sigma}_{eq}$ vs. strain $\overline{E}_{eq}$ for the mesoscopic scale, average equivalent stress $\widetilde{\Sigma}_{eq}$ vs. strain $\widetilde{E}_{eq}$ for individual grains in the mesoscopic scale and equivalent stress Σ_{eq} vs. strain E_{eq} relations for unit cells indicated in 4.1. As can be predicted, individual grains exhibit very different responses. Several grains with specific direction of lamella interfaces show very significant hardening. Interesting points are the existence of grains with very large strains and stresses, that are two times larger than the average values for the mesoscopic scale. Due to the interaction with the surrounding grains, individual grains in the mesoscopic scale show a conservative response as compared with the single crystalline model, which is typical of the mesoscopic scale. Extremely unique deformation behavior exhibiting softening and hardening disappeared in the grains of the mesoscopic scale. Figure 10 indicates average equivalent stress $\widetilde{\Sigma}_{eq}$ vs. strain $\widetilde{E}_{eq}$ for individual grains in mesoscopic scale and equivalent stress σ_{eq} vs. strain ε_{eq} relations for material points of specific grain in mesoscopic scale. All these suggest the importance of the evaluation of the deformation behavior of individual grains accounting for the interaction of the surrounding grains with different directional lamella interfaces to evaluate the local stress and strain that are indispensable for predicting the strength of the semicrystalline polymer.

Finally, we will discuss the mean stress which is the key parameter for evaluating the possibility of the onset of damages such as cavitation and crazing. Figure 11 indicates the distribution of mean stress σ_m in the amorphous phase and grain α in different deformation ranges indicated (1) to (5) in Fig.5. Figure 12 indicates the average mean stress $\widetilde{\Sigma}_m$ vs. equivalent strain $\widetilde{E}_{eq}$ relations for individual crystals of the mesoscopic scale and

average mean stress Σ_m vs. equivalent strain E_{eq} relations for unit cell. The high mean stress appears near the grain boundary with a large misalignment of the lamella interface direction. Very scattered distribution of mean stress depending on the location of material points in grain α can be seen. The mean stress in the mesoscopic scale is rather suppressed as compared with the unit cell case, which shows a tendency similar to that observed in the stress-strain relations in Fig. 9. Figure 13 indicates the average mean stress $\widetilde{\Sigma}_m$ vs. equivalent strain $\widetilde{E}_{eq}$ relations for crystal α and mean stress σ_m vs. equivalent strain ε_{eq} relations for the material point of grain α which suggest the large distribution as compared with the case of an equivalent stress. The mean stress is very strongly affected by the interaction with the surrounding grains, particularly, deformation constraint. Therefore, these results indicate the importance of the mesoscopic model in evaluating the mean stress in semicrystalline polymers.

5. Conclusion

We proposed a new multiscale model relating micro- to mesoscopic deformation behavior of semicrystalline polymers by employing homogenization method and clarified the characteristic deformation behavior of semicrystalline polymers. The main results obtained are as follows.

For unit cells

1. The microstructure of semicrystalline polymers exhibits highly anisotropic deformation behavior due to the preferential slip deformation of the chain slip system and the misalignment of lamella and chain directions.

2. Chain and lamella interface directions rotate to align the tensile direction as deformation increases. Depending on the initial direction of the interface, orientation hardening or softening occurs. When the chain direction aligns the maximum shear stress direction during deformation, the response exhibits orientation softening.

3. When the lamella interface normal is in the loading direction, the mean stress of the amorphous phase substantially increases, which may cause stress concentration and leads to microscopic fractures in semicrystalline polymers.

For the mesoscopic scale

4. The average responses of the mesoscopic scale are almost identical under different directional tensions that ensure an isotropy of the model and the validity of the present model.

5. Due to the interaction and orientation hardening of individual grains, the onset and propagation of local nonuniform deformation in the grain are observed, resulting in the onset and propagation of mesoscopic nonuniform deformation intercepting grains.

6. Equivalent stresses of individual grains are much more conserved than those of unit cells and suppress the unique response observed in the unit cells, which is closely associated with the interaction with the surrounding grains. The magnitude of mean stress exhibits a large scattering as compared with that of equivalent stress.

7. The local deformation behavior in the grain differs depending on the location of materials points that may exhibit more than 50% stress and strain; these should be considered in the evaluation of the strength of semicrystalline polymer.

Acknowledgements

Financial support from the Ministry of Education, Culture, Sports, Science and Technology of Japan is gratefully acknowledged.

References

1. Bowden PB, Young RJ. Deformation Mechanisms in Crystalline Polymers. Journal of Materials Science 1974; 9: 2034-2051

2. Lee BJ, Parks DM, Ahzi S. Micromechanical Modeling of Large Plastic Deformation and Texture Evolution in Semi-Crystalline Polymers. Journal of Mechanics and Physics of Solids 1993; 41: 1651-1687

3. Van Dommelen JAW, Parks DM., Boyce MC, Brekelmans WAM, Baaijens FPT. Micromechanical Modeling of the Elasto-Viscoplastic Behavior of Semi-Crystalline Polymers. Journal of the Mechanics and Physics of Solids 2003; 51: 519-541

4. Yashiro K, Kanai M, Tomita Y. AFM Study on Deformation Behavior of Polyethylene Lamella Structure by Means of In-situ Bending Test. Journal of the Society of Materials Science, Japan, 2004; submitted. (in Japanese)

5. Basset DC, Hodge AM. On the Morphology of Melt-Crystallized Polyethylene I. Lamellar Profiles. Proceedings of the Royal Society of London A, 1981; 377: 25-37

6. Higa Y, Tomita Y. Computational Prediction of Mechanical Properties of Nickel-Based Superalloy with Gamma Prime Phase Precipitates. Advance Materials and Modeling of Mechanical Behavior, 1999; III: 1061-1066, Fleming Printing Ltd.

7. Peirce D, Asaro RJ, Needleman A. Material Rate Dependence and Localized Deformation in Crystalline Solids. Acta Metallurgica 1983; 31: 1951-1976

8. Tomita Y, Adachi T, Tanaka S. Modeling and Application of Constitutive Equation for Glassy Polymer Based on Nonaffine Network Theory. European Journal of Mechanics - A/Solids 1997; 16: 745-755

9. Hutchinson JW. Bounds and Self-Consistent Estimates for Creep of Polycrystalline Materials. Proceedings of the Royal Society of London A 1976; 348: 101-127

10. Uchida M, Tomita Y. Deformation of Crystalline Polymers Containing Amorphous Phase. Proceedings of CMD200 , 2003; 111-112 (in Japanese)

11. Argon AS. A Theory for the Low-Temperature Plastic Deformation of Glassy Polymers. Philosophical Magazine 1973; 28: 839-865

12. Boyce MC, Parks DM, Argon AS. Large Inelastic Deformation of Glassy Polymers, Part I: Rate Dependent Constitutive Model. Mechanics of Materials 1988; 7: 15-33

13. Arruda EM, Boyce MC. A Three-Dimensional Constitutive Model for the Large Stretch Behavior of Rubber Elastic Materials. Journal of the Mechanics and Physics of Solids. 1993; 41: 389-412

14. Tomita Y, Uchida M. Characterization of Micro- to Macroscopic Deformation Behavior of Amorphous Polymer with Heterogeneous Distribution of Microstructures. International Journal of Mechanical Science 2003; 45:1703-1716

15. Tomita Y, Wei Lu. Characterization of Micro- to Macroscopic Response of Polymers Containing Second-Phase Particles Under Macroscopically Uniform Deformation. International Journal of Solids & Structures 2002, 39: 3409-3428

Figure Captions

Figure 1. Computational model
(a) Unit cell model, (b) mesoscopic model

Figure 2. Deformation behavior of unit cells under different directional tensions.
(a) Equivalent stress Σ_{eq}, (b) direction of chain axis θ_c, and (c) direction of lamella interface θ_i vs.. equivalent strain E_{eq}

Figure 3. Deformation behavior of unit cells under different directional tensions
(a) Mean stress Σ_m in amorphous phase and (b) mean stress in crystalline phase Σ_m vs.. equivalent strain E_{eq}

Figure 4. Deformation behavior of microstructure under different directional tensions
Thick and thin lines indicate unit cell and finite element discretizations, respectively. The gray lines in crystalline phase indicate the direction of the chain axis.

Figure 5. Relationships between average equivalent stress $\overline{\Sigma}_{eq}$ and strain $\overline{E}_{eq}$ in mesoscopic scale for different directional tensions

Figure 6. Effect of crystallinity on average equivalent stress $\overline{\Sigma}_{eq}$ and strain $\overline{E}_{eq}$ relations for mesoscopic scale.

Figure 7. Equivalent strain rate $\dot{\varepsilon}_{eq}$ distribution on mesoscopic scale at different deformation stages indicated as (1) to (5) in Fig.5

Figure 8. Deformation behavior of specific materials points indicated as A, B, C and D in Fig.7 at different deformation stages as indicated (1) to (5) in Fig.5
The thin lines indicate finite element discretization. The gray lines in crystalline phase denote the direction of chain axis.

Figure 9. Average equivalent stress $\overline{\Sigma}_{eq}$ vs. strain $\overline{E}_{eq}$ for mesoscopic scale, average equivalent stress $\widetilde{\Sigma}_{eq}$ vs. strain $\widetilde{E}_{eq}$ for individual grains and equivalent stress Σ_{eq} vs. strain E_{eq} relations for unit cells

Figure 10. Average equivalent stress $\widetilde{\Sigma}_{eq}$ vs. strain $\widetilde{E}_{eq}$ for individual grains in mesoscopic scale and equivalent stress σ_{eq} vs. strain ε_{eq} relations for material points of specific grain in mesoscopic scale

Figure 11. Distribution of mean stress σ_m in amorphous phase and grain α at different deformation ranges as indicated (1) to (5) in Fig.5

Figure 12. Average mean stress $\widetilde{\Sigma}_m$ vs. equivalent strain $\widetilde{E}_{eq}$ relations for individual crystal of mesoscopic scale and average mean stress Σ_m vs. equivalent strain E_{eq} relations for unit cell.

Figure 13. Average mean stress $\widetilde{\Sigma}_m$ vs. equivalent strain $\widetilde{E}_{eq}$ relations for crystal α of mesoscopic scale and mean stress σ_m vs. equivalent strain ε_{eq} relations for material point of crystal α.

Fig.1

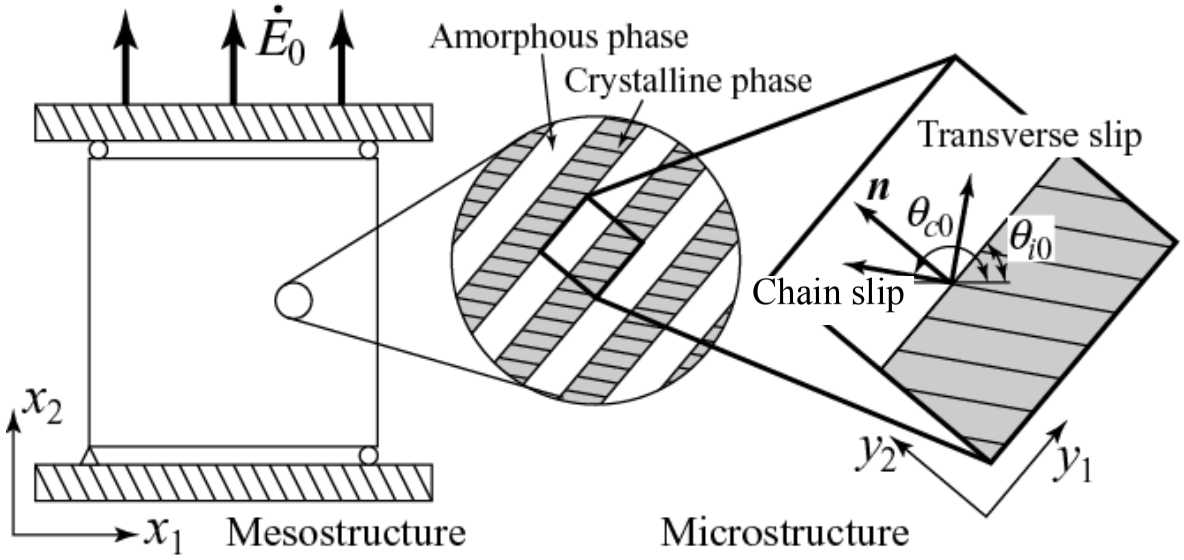

(a) Unit cell model

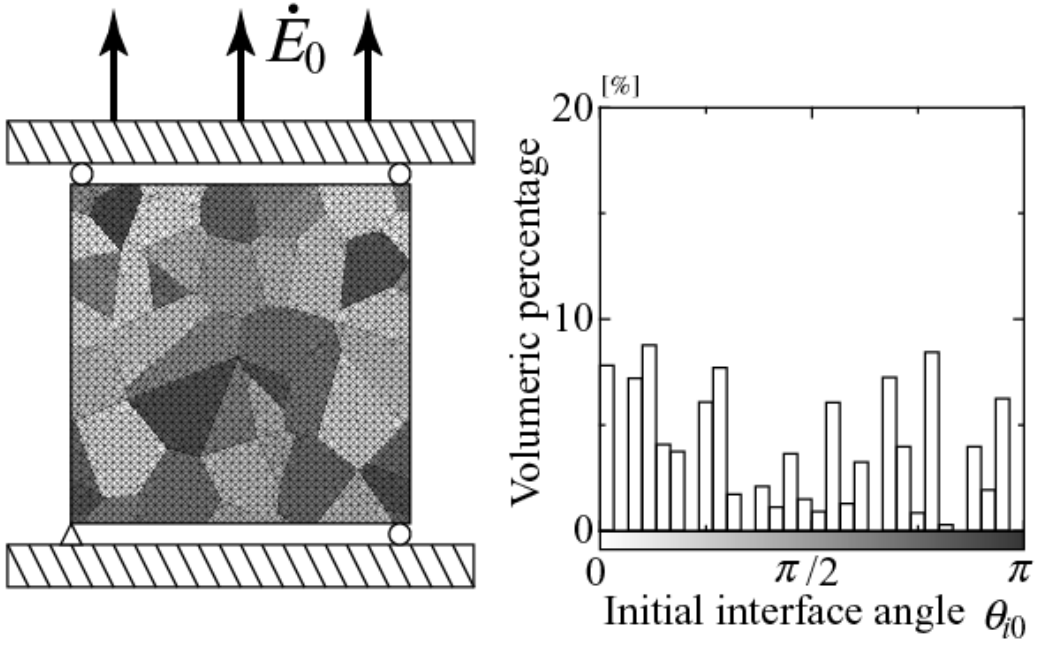

(b) Mesoscopic model

Fig.2

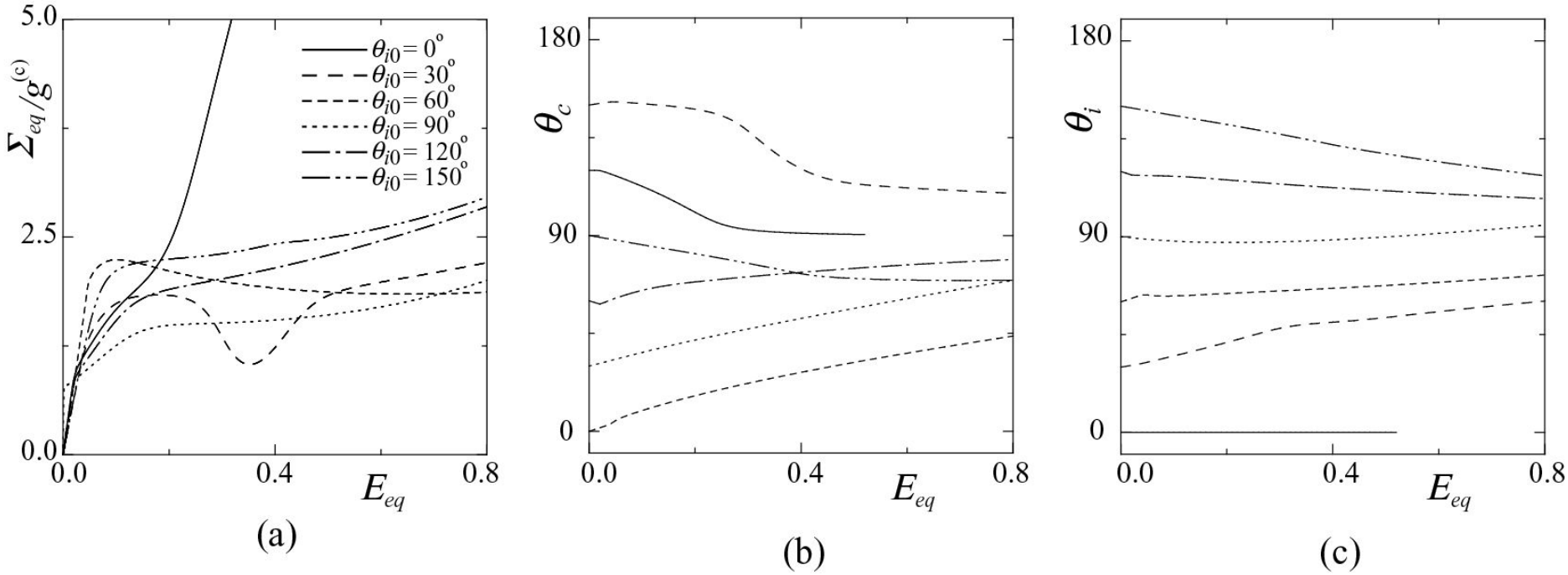
5.0
2.5
0.0
0.0
0.4
0.8
E_{eq}
$\Sigma_{eq}/g^{(c)}$
θ_{i0}= 0°
θ_{i0}= 30°
θ_{i0}= 60°
θ_{i0}= 90°
θ_{i0}= 120°
θ_{i0}= 150°
(a)
180
90
0
θ_c
(b)
θ_i
(c)

Fig.3

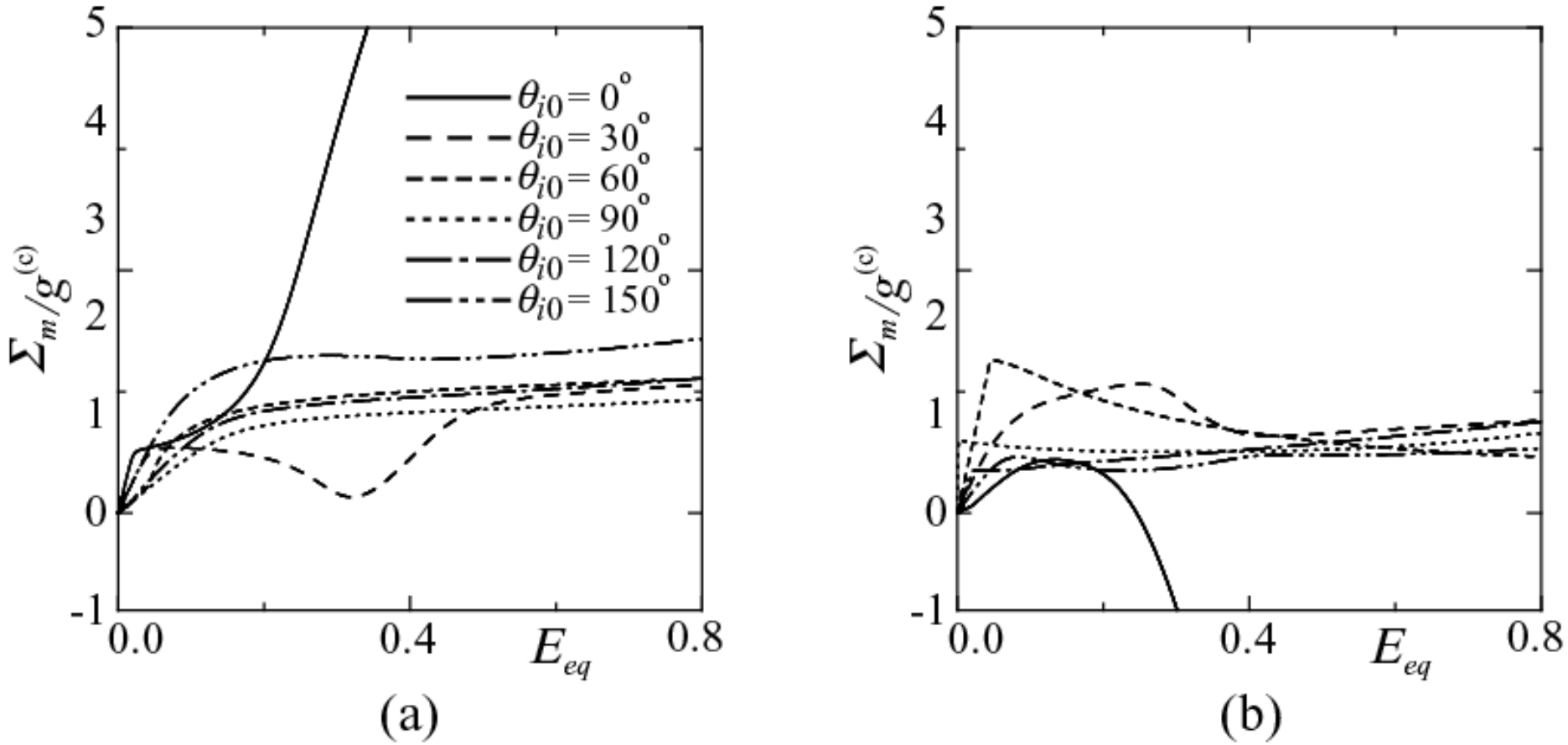
5
4
3
2
1
0
-1
0.0
0.4
0.8
E_{eq}
$\Sigma_m/g^{(c)}$
$\theta_{i0}=0^{\circ}$
$\theta_{i0}=30^{\circ}$
$\theta_{i0}=60^{\circ}$
$\theta_{i0}=90^{\circ}$
$\theta_{i0}=120^{\circ}$
$\theta_{i0}=150^{\circ}$
(a)
(b)

Fig.4

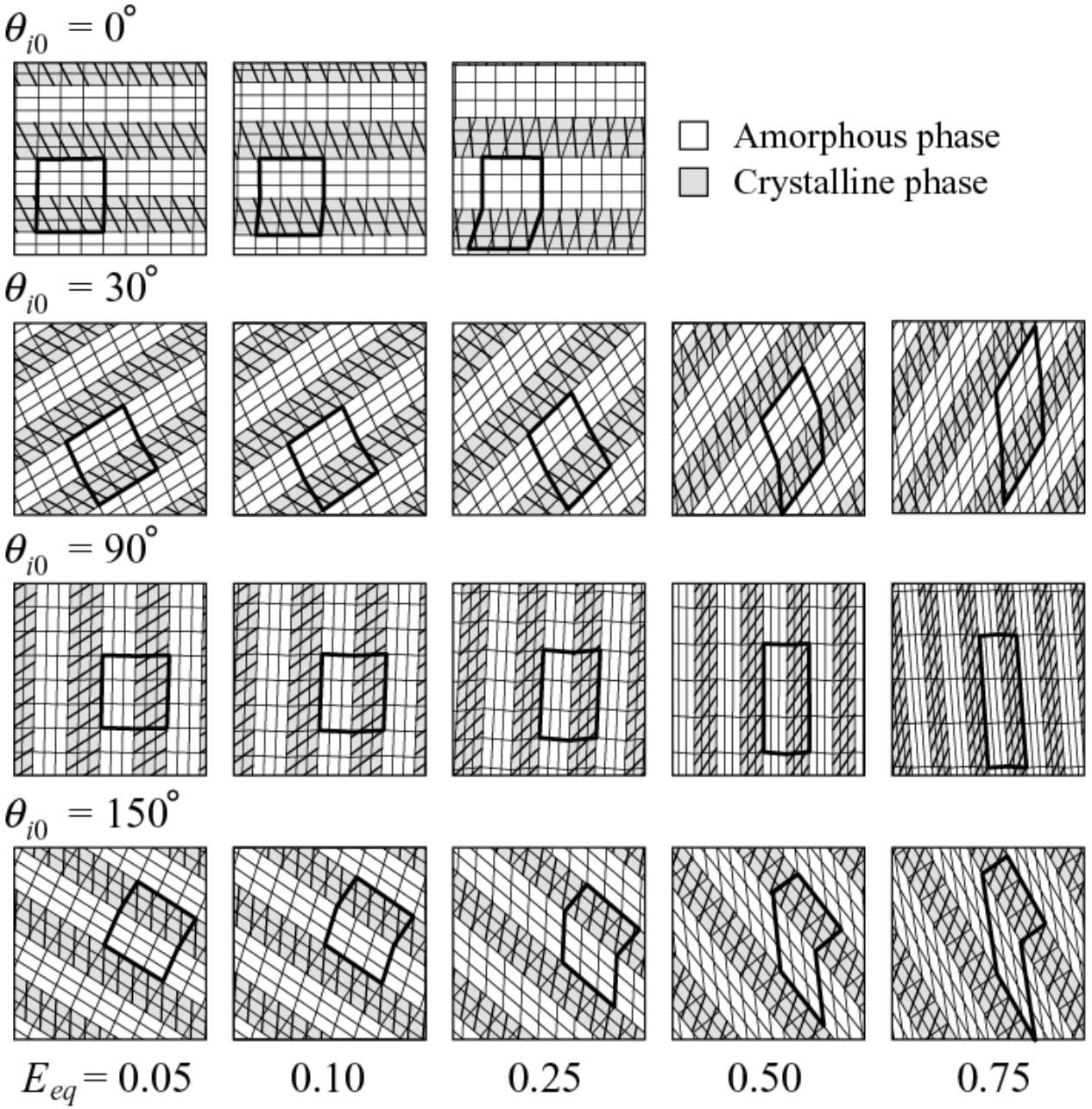
$\theta_{i0} = 0^\circ$
$\theta_{i0} = 30^\circ$
$\theta_{i0} = 90^\circ$
$\theta_{i0} = 150^\circ$
Amorphous phase
Crystalline phase
$E_{eq} = 0.05$
0.10
0.25
0.50
0.75

Fig.5

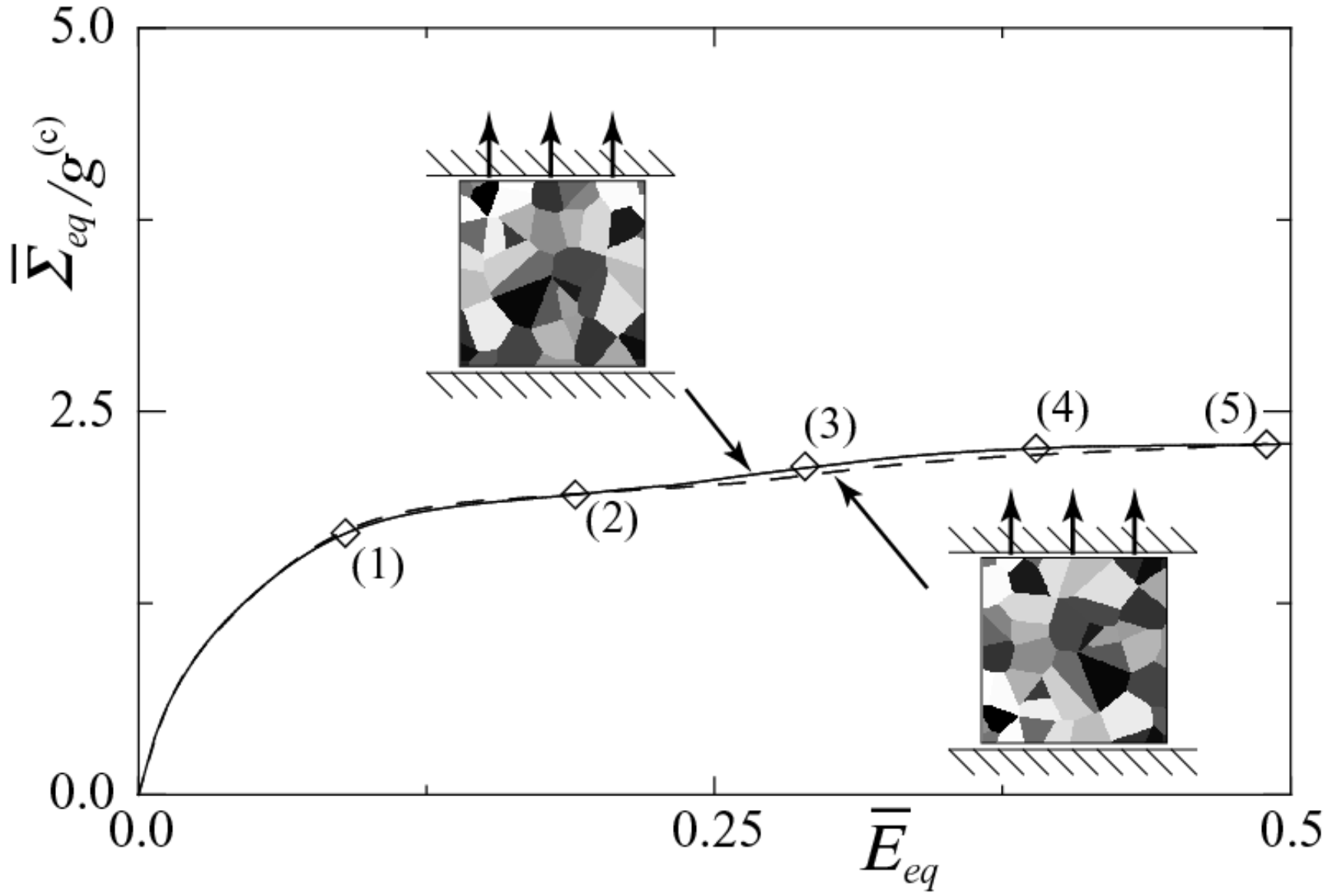

Fig.6

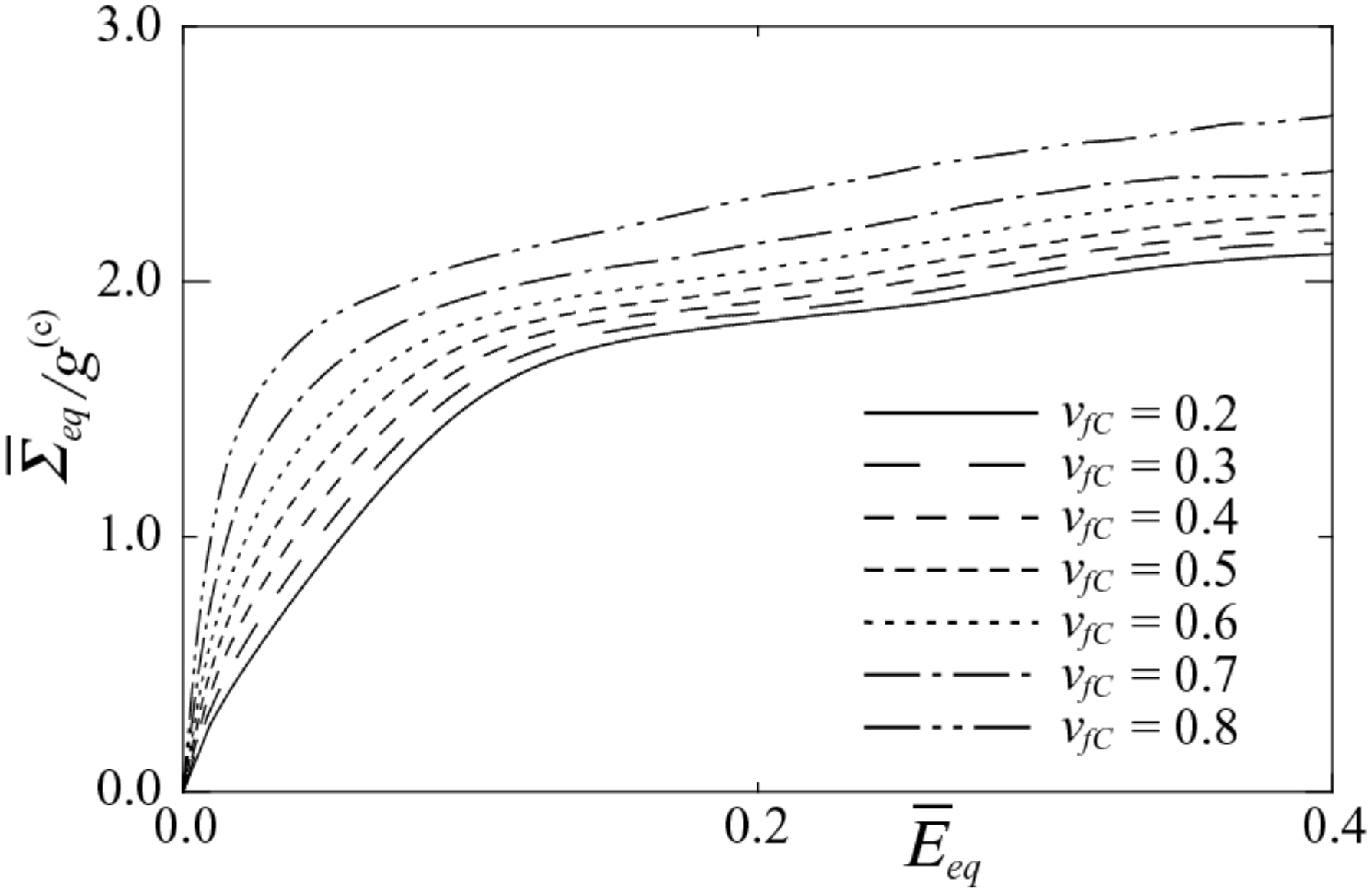
3.0
2.0
1.0
0.0
0.0
0.2
0.4
$\overline{\Sigma}_{eq}/g^{(c)}$
$\overline{E}_{eq}$
$\nu_{fC} = 0.2$
$\nu_{fC} = 0.3$
$\nu_{fC} = 0.4$
$\nu_{fC} = 0.5$
$\nu_{fC} = 0.6$
$\nu_{fC} = 0.7$
$\nu_{fC} = 0.8$

Fig.7

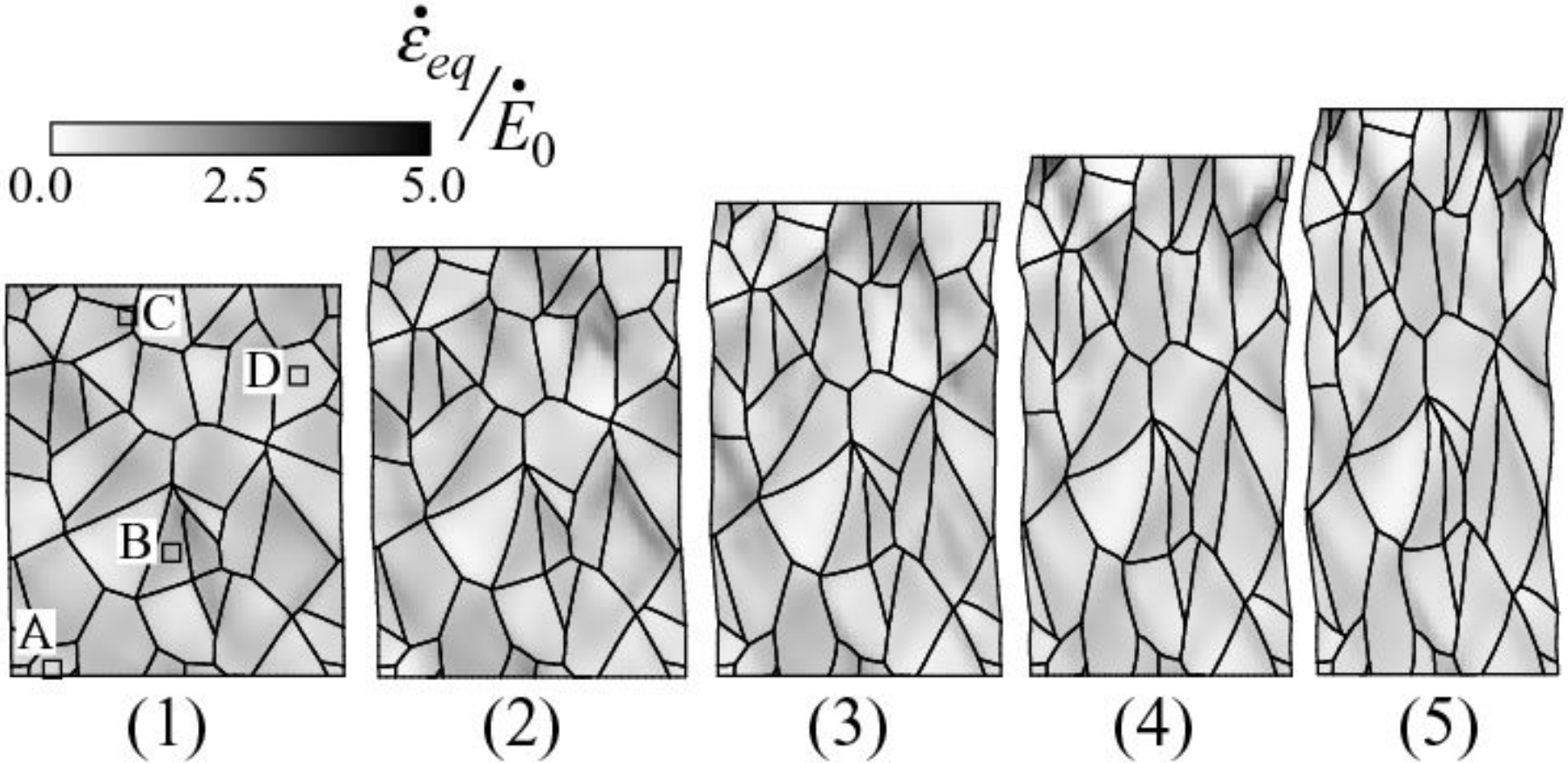

Fig.8

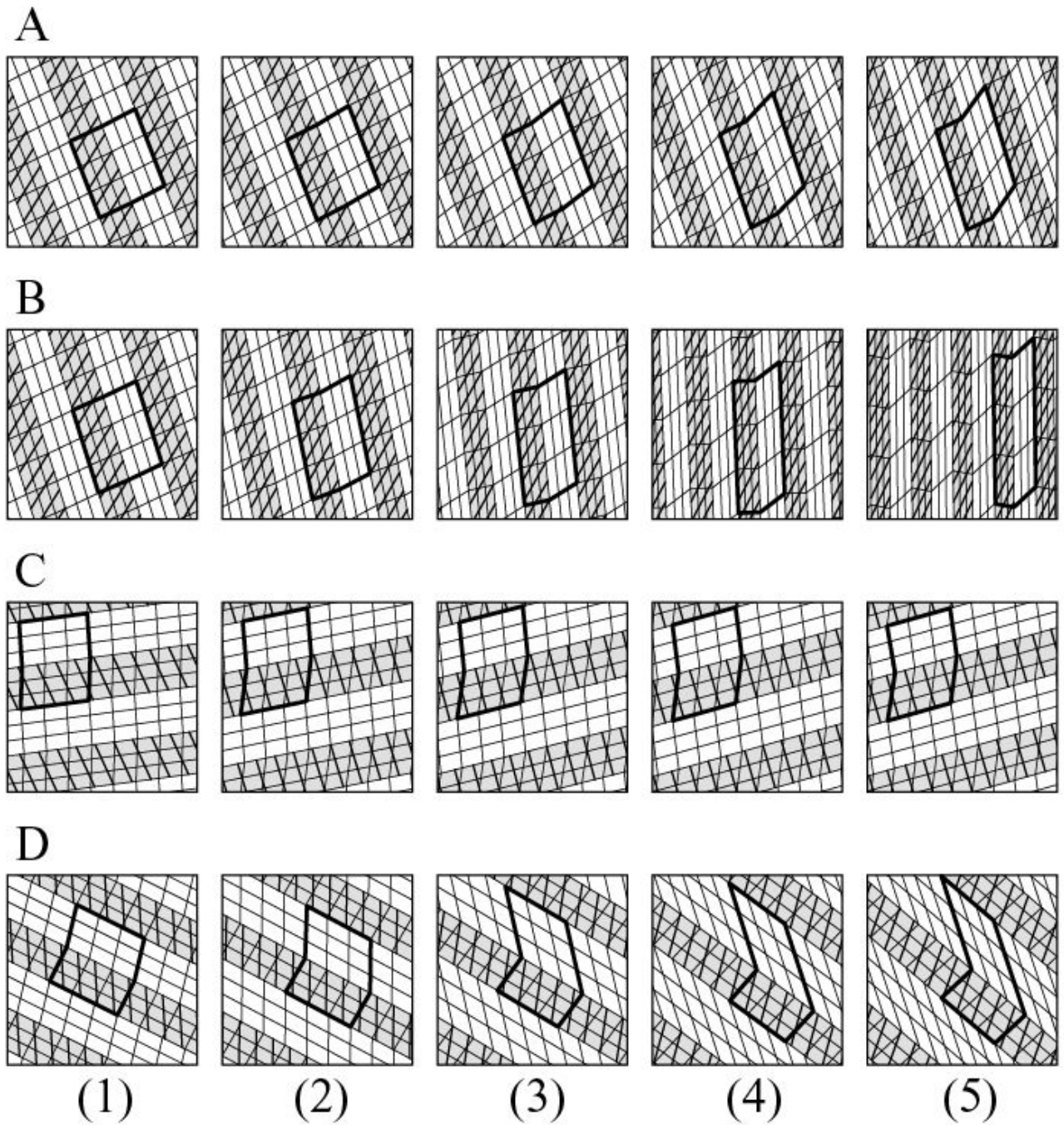

Fig.9

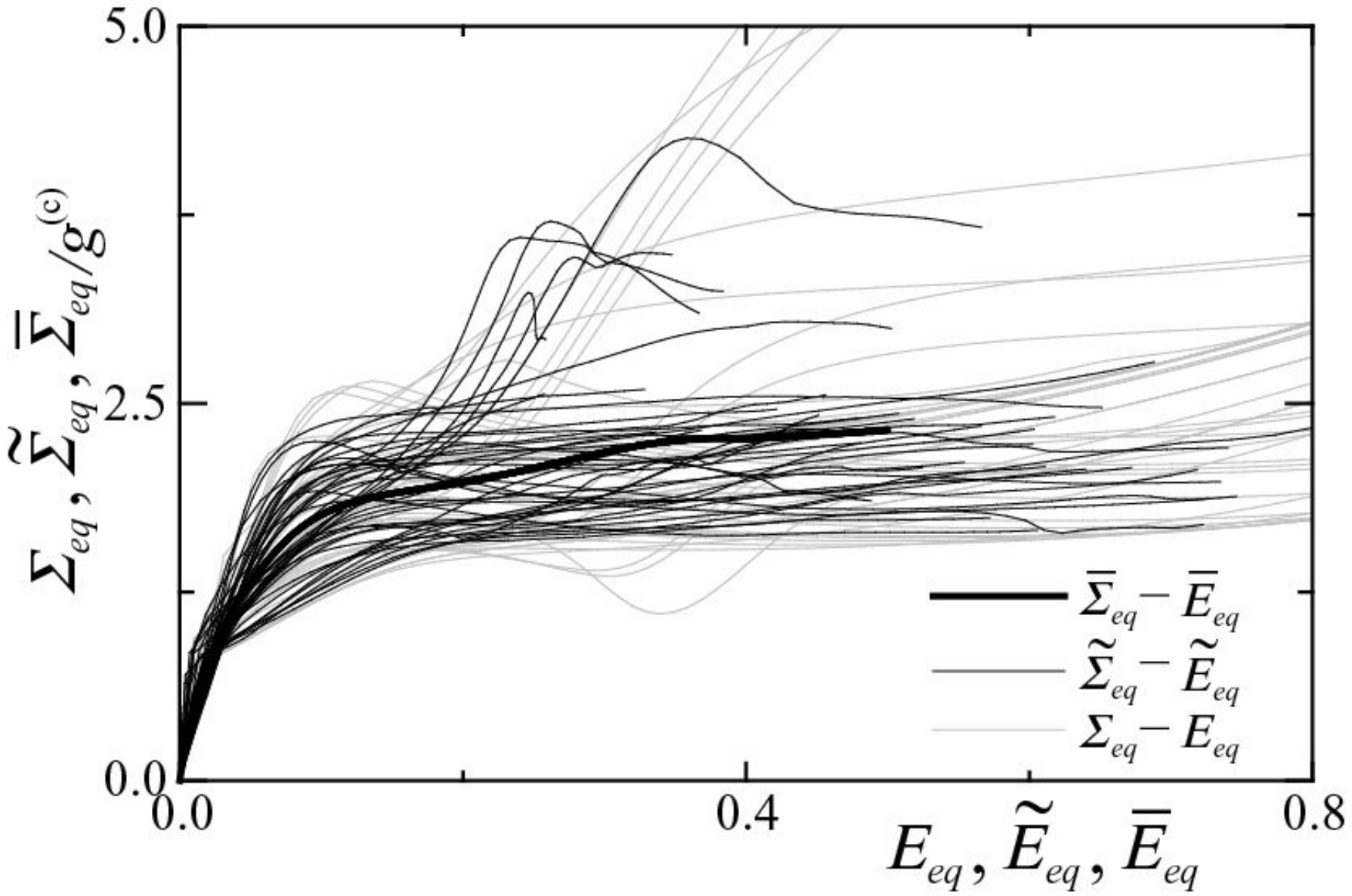
5.0
2.5
0.0
0.0
0.4
0.8
$\Sigma_{eq}, \tilde{\Sigma}_{eq}, \bar{\Sigma}_{eq}/g^{(c)}$
$E_{eq}, \tilde{E}_{eq}, \bar{E}_{eq}$
$\bar{\Sigma}_{eq} - \bar{E}_{eq}$
$\tilde{\Sigma}_{eq} - \tilde{E}_{eq}$
$\Sigma_{eq} - E_{eq}$

Fig.10

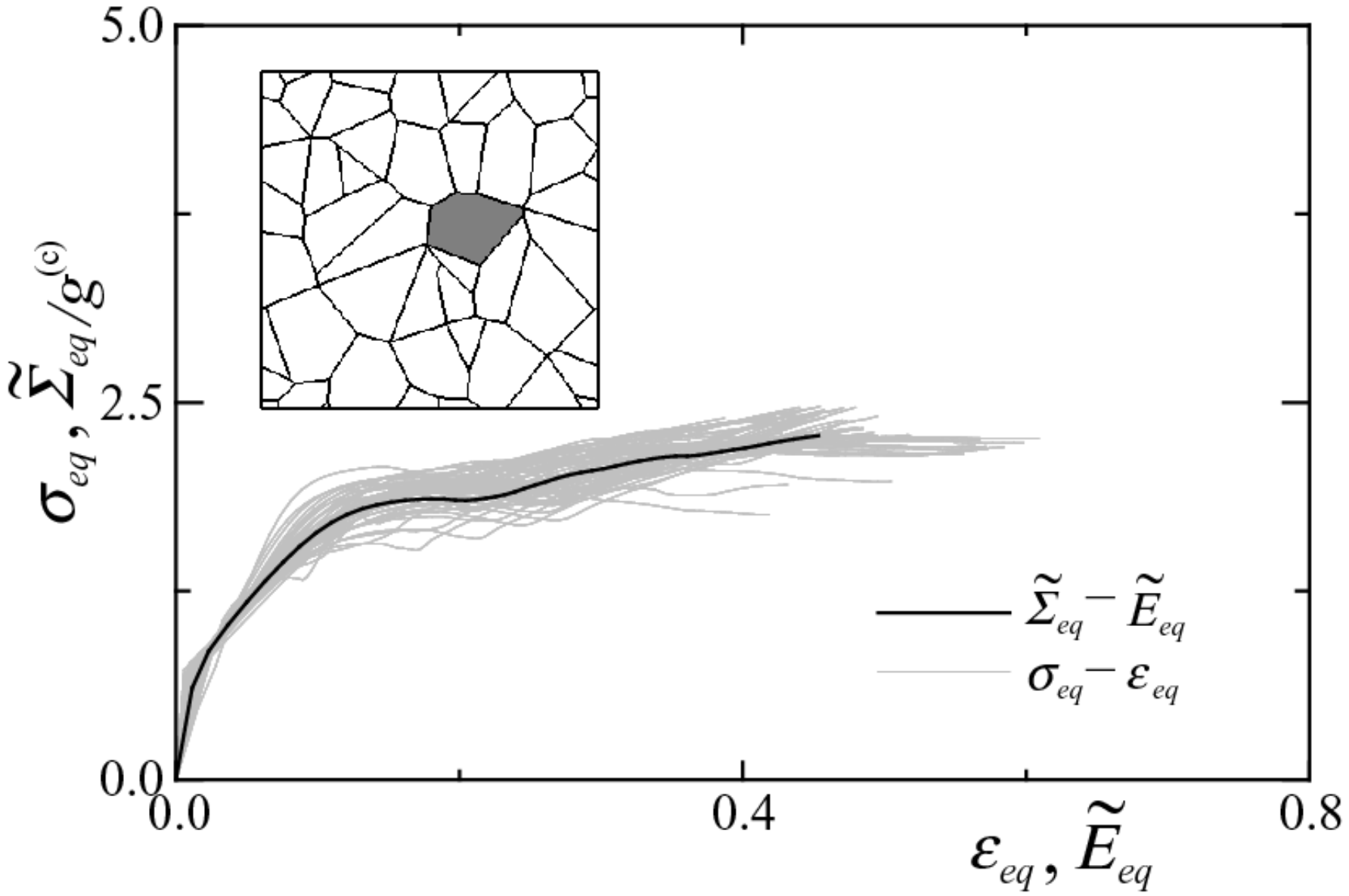
5.0
2.5
0.0
0.0
0.4
0.8
$\sigma_{eq}, \tilde{\Sigma}_{eq}/g^{(c)}$
$\varepsilon_{eq}, \tilde{E}_{eq}$
$\tilde{\Sigma}_{eq} - \tilde{E}_{eq}$
$\sigma_{eq} - \varepsilon_{eq}$

Fig.11

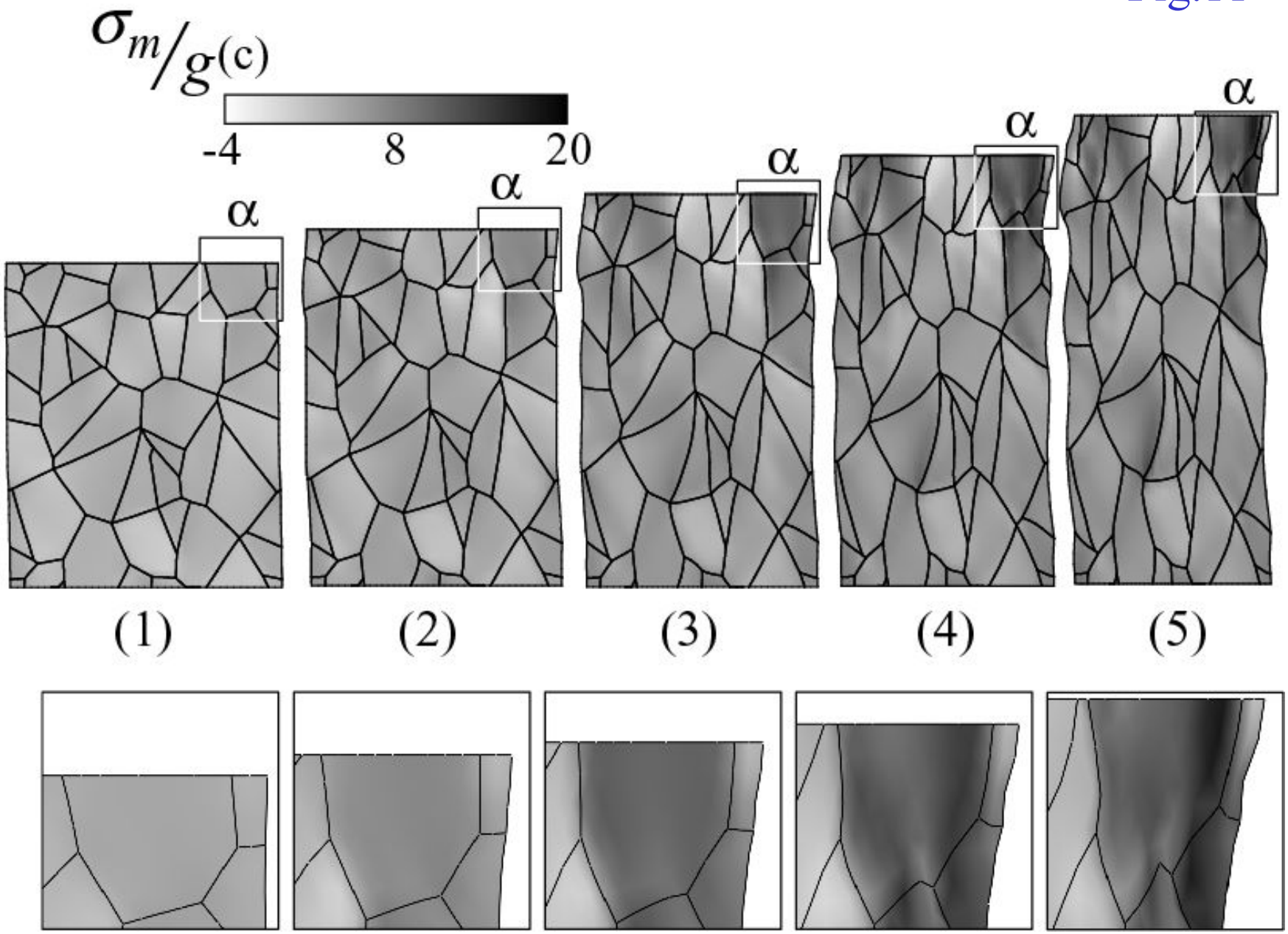

Fig.12

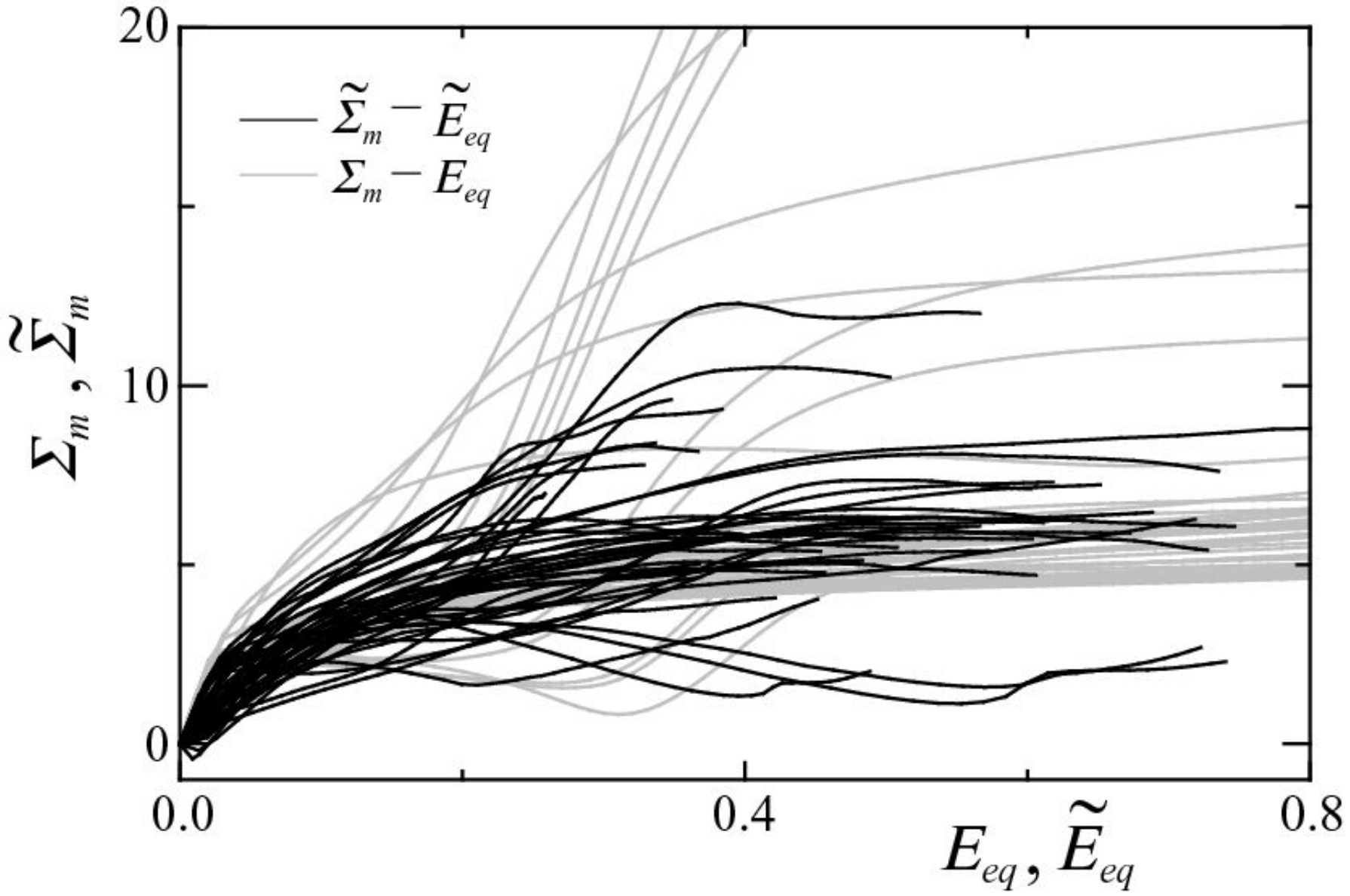
20
10
0
0.0
0.4
0.8
$\widetilde{\Sigma}_m - \widetilde{E}_{eq}$
$\Sigma_m - E_{eq}$
Σ_m , $\widetilde{\Sigma}_m$
E_{eq} , $\widetilde{E}_{eq}$

Fig.13

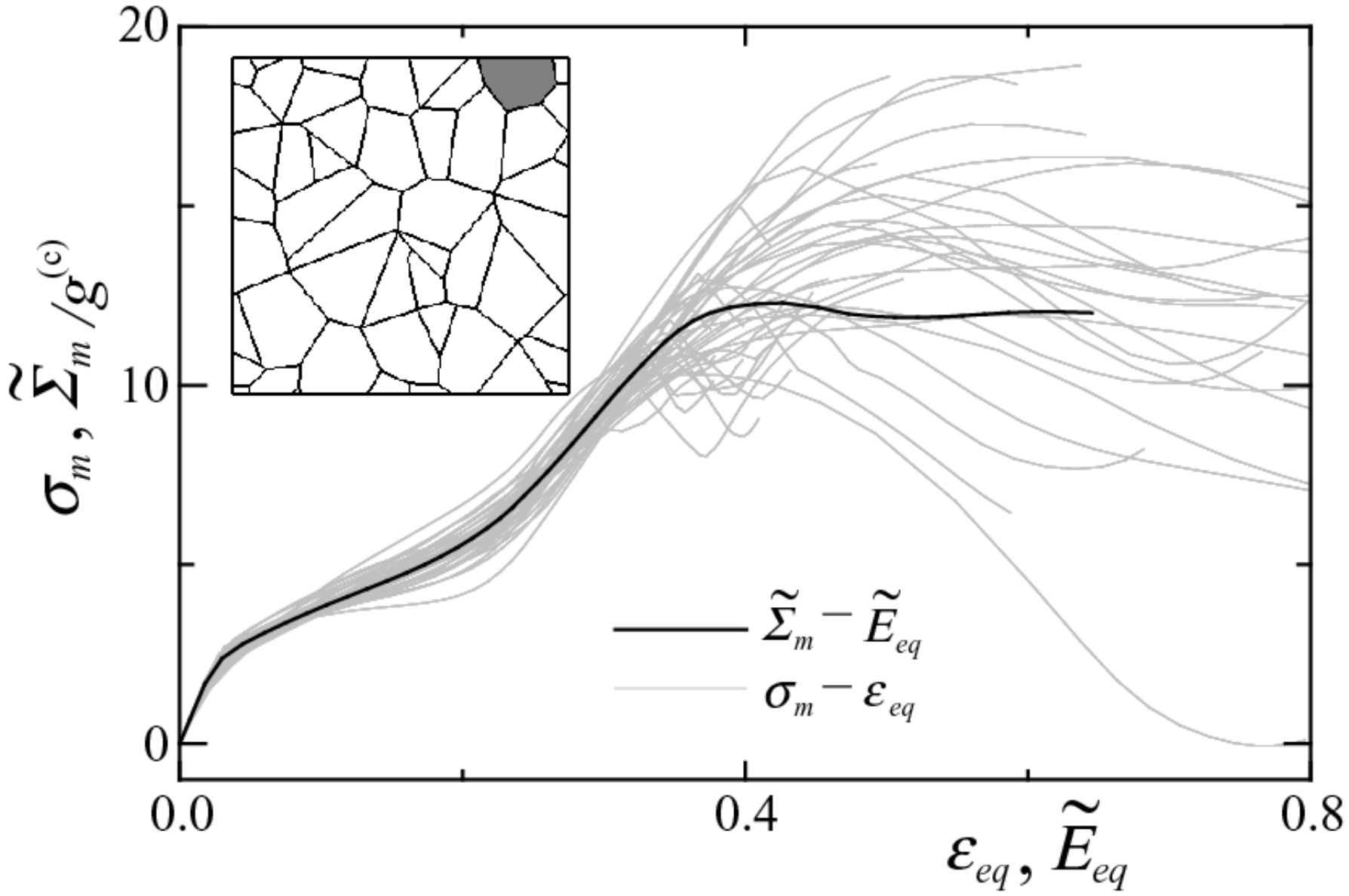
20
10
0
0.0
0.4
0.8
$\tilde{\Sigma}_m / g^{(c)}$
σ_m , $\tilde{\Sigma}_m$
ε_{eq} , $\tilde{E}_{eq}$
$\tilde{\Sigma}_m - \tilde{E}_{eq}$
$\sigma_m - \varepsilon_{eq}$